Two Different Pathways toward Self-aggregation under Radiative-convective Equilibrium between SCALE and VVM

Jin-De Huang[1], Ching-Shu Hung[2], Chien-Ming Wu[1], and Hiroaki Miura[2]

1. Department of Atmospheric Sciences, National Taiwan University, Taipei, Taiwan
2. Department of Earth and Planetary Science, Graduate School of Science, The University of Tokyo, Tokyo, Japan

Corresponding authors: Chien-Ming Wu (mog@as.ntu.edu.tw)

Key points:

- Two CRMs, SCALE and VVM, undergo different transitions toward convective self-aggregation despite the same sea surface temperature.
- Radiative cooling in SCALE dominates the development of self-aggregation, while convection in moist areas drives self-aggregation in VVM.
- The different pathways to self-aggregation are associated with different changes in the scale of convective clouds.

Abstract

Two cloud-resolving models (SCALE and VVM) take different pathways toward convective self-aggregation under a radiative-convective equilibrium condition, although the model setups are the same. The physical processes driving the development of self-aggregation in SCALE and VVM, respectively, correspond to the mechanisms for self-aggregation in cold and warm climate states discussed in a previous study. Analyses in the moisture space show that radiative cooling in the dry area mainly drives the aggregation in SCALE, while subsidence induced by the convection in the moist region dominates in VVM. The transition of the convective circulation from convective scale to mesoscale is found on the isentropic diagram in VVM, but this transition is unclear in SCALE. The convective clouds with larger sizes are rare in SCALE. The frequent occurrence of larger convective clouds efficiently drives self-aggregation from the moist area in VVM. These results provide a new insight to understand convective self-aggregation among models.

Plain Language Summary

A variety of deep convective clouds is found in the tropics, and they sometimes form clusters. Previous studies have found that the mechanisms for the onset of the clustered convection are very different in warmer and colder sea surface temperature conditions in idealized numerical experiments. We discover that the mechanisms can be different among the two models even though the sea surface temperature is the same. The clustering in one model is driven by the radiative processes in the region without convection. In the other model, the clustering is controlled by circulation from the region with larger convective clouds. This study shows that the different mechanisms for the onset of the clustered convection among models are related to how the model simulates deep convective clouds and their properties. This result improves our understanding of the clustered convection in the models.

1 Introduction

Radiative convective equilibrium (RCE) is known as a conceptual model for understanding tropical climate (Manabe and Strickler 1964). In this model, moist convection is essential to balance the radiative cooling and the surface warming to reach an equilibrium climate state with a statically stable thermodynamic structure. This concept has been applied using cloud-resolving models (CRMs), and the models reach equilibrium states with smaller convective regions surrounded by larger and wider dry subsiding regions (Nakajima and Matsuno 1988; Held et al. 1993; Tompkins and Craig 1998; Bretherton et al. 2005; Muller and Held 2012; Wing and Emanuel 2014; Yanase and Takemi 2018). This process, which is called convective self-aggregation, drastically changes the radiation balance of the domain, and changes due to self-aggregation would be potential impacts on the climate sensitivity. For example, Coppin and Bony (2015) investigated the dependence of self-aggregation on surface temperature using an atmospheric general circulation model. At low sea surface temperature (SST), the radiative cooling in dry areas or low-cloud region drives large-scale subsidence. The expansion of this subsidence region forces convection to aggregate in the regions with weak subsidence. On the other hand, at high SST, deep convection develops and then induces strong surface wind, which leads to enhanced surface enthalpy flux in the adjacent region. The enhanced surface flux will favor the subsequent development of deep convection in similar areas, and this feedback dominates the development of self-aggregation. Their results suggested that the critical mechanism leading to self-aggregation can be different under different climate states.

The RCE Model Intercomparison Project (RCEMIP) was organized by Wing et al. (2018) to investigate the role of clouds and self-aggregation in the climate sensitivity. Wing et al. (2020) showed that the horizontal convection distribution and the vertical cloud fraction

considerably vary across CRMs despite homogeneous 300 K SST, and the dependence of self-aggregation on SST is diverse. Different equilibrium states among CRMs are driven by convection even though the same initial conditions and SST are given. The spread results in RCEMIP reveal that self-aggregation can be sensitive to the treatment of convective processes, such as the cloud microphysics and the radiation. The distinct responses of self-aggregation to warming SST in RCEMIP raise an important question of whether or not the critical mechanism driving self-aggregation is consistent in CRMs under the same SST.

This study investigates the crucial process leading to self-aggregation using two CRMs, and the experimental setups follow the RCEMIP protocol (Wing et al. 2018), except for the domain size. The equilibrium state with self-aggregation is obtained with a medium domain size to reduce the computational costs. The analysis in the moisture space is used to evaluate the differences in the equilibrium state, and the isentropic analysis (Pauluis et al. 2013) is applied to examine the time evolution of the convective structures as self-aggregation develops. Section 2 describes the two models and the experimental setup, and section 3 discusses the different pathways towards convective self-aggregation. The summary and discussion are in section 4.

2 Models and Experiment Design

2.1 Model description

2.2.1 SCALE

The first atmospheric model used in this study is a regional model constructed with Scalable Computing for Advanced Library and Environment (SCALE, Version 5.3.6; Nishizawa et al., 2015; Sato et al., 2015). The model is governed by the three-dimensional fully compressible non-hydrostatic equations, which predicts the three-dimensional momentum (ρu, ρv, ρw), total density (ρ), mass-weighted potential temperature ($\rho\theta$), and mass concentration of tracers (ρq_s). The θ here is not the conventional potential temperature for dry air, but the corresponding value for total air, considering water content. A six-class single-moment bulk-type microphysics scheme is used in this study (Tomita 2008). The subgrid-scale turbulent process is parameterized through the Smagorinsky-Lilly type first-order closure scheme (Brown et al., 1994; Scotti et al., 1993), and surface fluxes are calculated by a bulk method using a universal function (Beljaars and Holtslag 1991; Wilson 2001). The radiative processes are treated with a k-distribution-based broadband radiation transfer model (Mstrn-X, Sekiguchi and Nakajima 2008).

2.2.2 VVM

The other model used in this study is the vector vorticity equation cloud-resolving model (VVM) developed by Jung and Arakawa (2008). Horizontal components of anelastic vorticity equations are predicted in the VVM, and velocities are diagnosed through solving a three-dimensional elliptic equation. The use of the vorticity equations eliminates pressure gradient force and inherently links the dynamics and the thermodynamics in the governing equations. The direct couple in the equations can better capture local circulations associated with strong thermal gradients, such as the land-sea breeze. The radiation model (RRTMG,

Iacono et al. 2008), the land surface model (Noah LSM, Chen and Dudhia 2001), the predicted particle properties microphysical scheme (Morrison and Milbrandt 2015; Huang and Wu 2020), and the block topography (Wu and Arakawa 2011; Chien and Wu 2016) has been implemented in the VVM. With the inclusion of these physical processes, the model has been used in many studies; for example, unified parameterization (Arakawa and Wu 2013; Wu and Arakawa 2014), stratocumulus dynamics (Tsai and Wu 2016), afternoon thunderstorms (Kuo and Wu 2019), impacts of land surface heterogeneity (Wu et al. 2019; Wu and Chen 2020), cloud-aerosol interactions (Chang et al. 2021), coastal convection during summer monsoon onset (Chen et al. 2019), and the aggregated convection (Tsai and Wu 2017; Chen and Wu 2019).

2.2 Experiment design

VVM and SCALE used their default physics settings with the same experimental settings following the RCEMIP protocol (Wing et al. 2018). The simulations are initialized from an analytically approximated sounding of the moist tropics (Dunion 2011) and integrated with a fixed SST of 300 K for 50 days with hourly data outputs. The domain size is 384×384 km^2 with a 2-km horizontal resolution to have minimal costs. Yanase et al. (2020) investigated and suggested that 384 km is the minimum size for self-aggregation in SCALE with the 2-km resolution.

3 Result

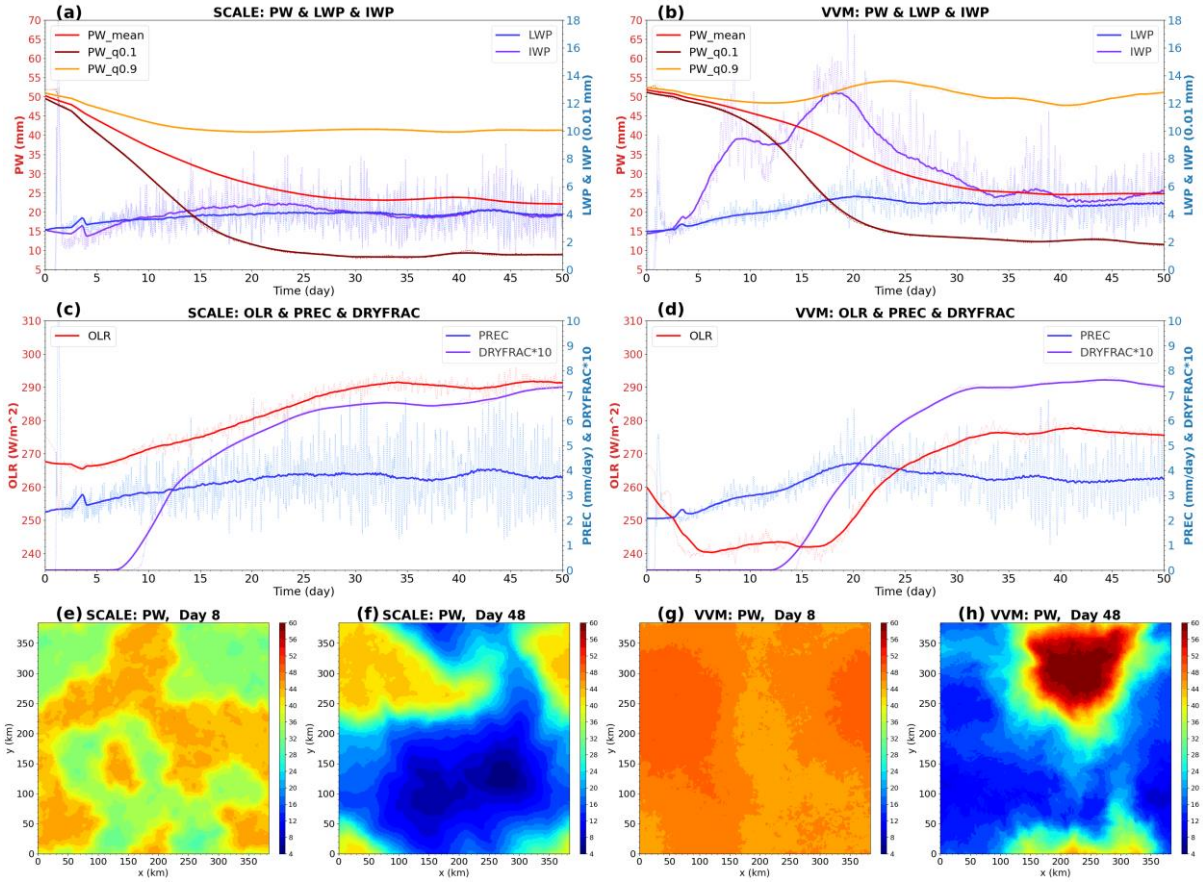

Fig. 1. The time evolutions of domain-averaged precipitable water (PW, PW_mean), liquid water path (LWP), ice water path (IWP), and the averages of moistest 10 % PW (PW_q0.9) and driest 10 % PW (PW_q0.1) for SCALE (a) and VVM (b). The time series of domain-averaged outgoing longwave radiation (OLR), precipitation (PREC), and dry area fraction (DRYFRAC) for SCALE (c) and VVM (d). The solid lines represent 5-day moving average, and the dashed lines are shown without temporally smoothing. The horizontal distribution of daily averaged PW for SCALE (e, f) and VVM (g, h) on day 8 and day 48.

3.1 Overall behaviors of two models

The convective aggregation can be identified through the evolution of precipitable water (PW), as shown in Fig. 1. The evolution of 10 and 90 percentiles of PW show that the horizontal contrast of PW increases as time proceeded, which indicates the development of

self-aggregation. Both models roughly reach a quasi-steady state after day 40 with the mean of 25 mm PW. Although the domain-averaged PW and precipitation rate are similar, the structure of convection is different in the two models, as shown in the horizontal distribution of PW on day 48 (Fig. 1f and 1h). In SCALE, a moderate moist patch with a typical value of about 42 mm PW is surrounded by a substantially dry area with around 4 mm PW. On the other hand, a dense, moist patch where PW is greater than 60 mm is encompassed with a moderate dry patch with about 12 mm PW in VVM. Throughout the transition toward the self-aggregated state, the liquid water path (LWP) similarly evolves in both models. Still, the evolution of the ice water path (IWP) is different between SCALE and VVM. IWP in VVM significantly increases before day 20 and then settles to equilibrium, while SCALE has a smaller temporal variation of IWP during the development of self-aggregation. These results hint at different evolutions of convective structures toward aggregation. This difference in the evolutions can also be visualized by the outgoing longwave radiation (OLR). VVM takes lower domain-averaged OLR of about 240 W m^{-2} between 5 and 15 days, and OLR then significantly increases to roughly 280 W m^{-2}. In contrast, the domain-averaged OLR of SCALE steadily increases to about 290 W m^{-2} without a clear decrease like VVM. In the equilibrium state, the OLR of SCALE is 15 W m^{-2} greater than that of VVM, which implies that radiative processes are more efficient in SCALE. The dry fraction (DRYFRAC), defined as the fraction of areas where precipitable water lower than 30 mm (Yanase et al. 2020), also provides a different perspective about the evolution of the two models. DRYFRAC in VVM starts its increase at day 13, accompanied by the decay of IWP and the recovery of OLR. This feature also suggests that the aggregation in VVM develops with changes in the convective structures. On the other hand, DRYFRAC of SCALE starts increasing with gentle changes of IWP and OLR at day 8. The daily-averaged PW at day 8 in SCALE (Fig. 1e) shows that the expansion of the dry region already develops and can eventually lead to aggregation. The horizontal moisture variation is

smaller at day 8 in VVM (Fig. 1g). It is notable that the PW of the most humid region in SCALE at day 8 is similar to that at day 48, while the moistest region in VVM becomes moister at day 48 compared to day 8. The above results reveal that the development of self-aggregation undergoes very different ways in two models even though they eventually reach the equilibrium with the convective aggregation.

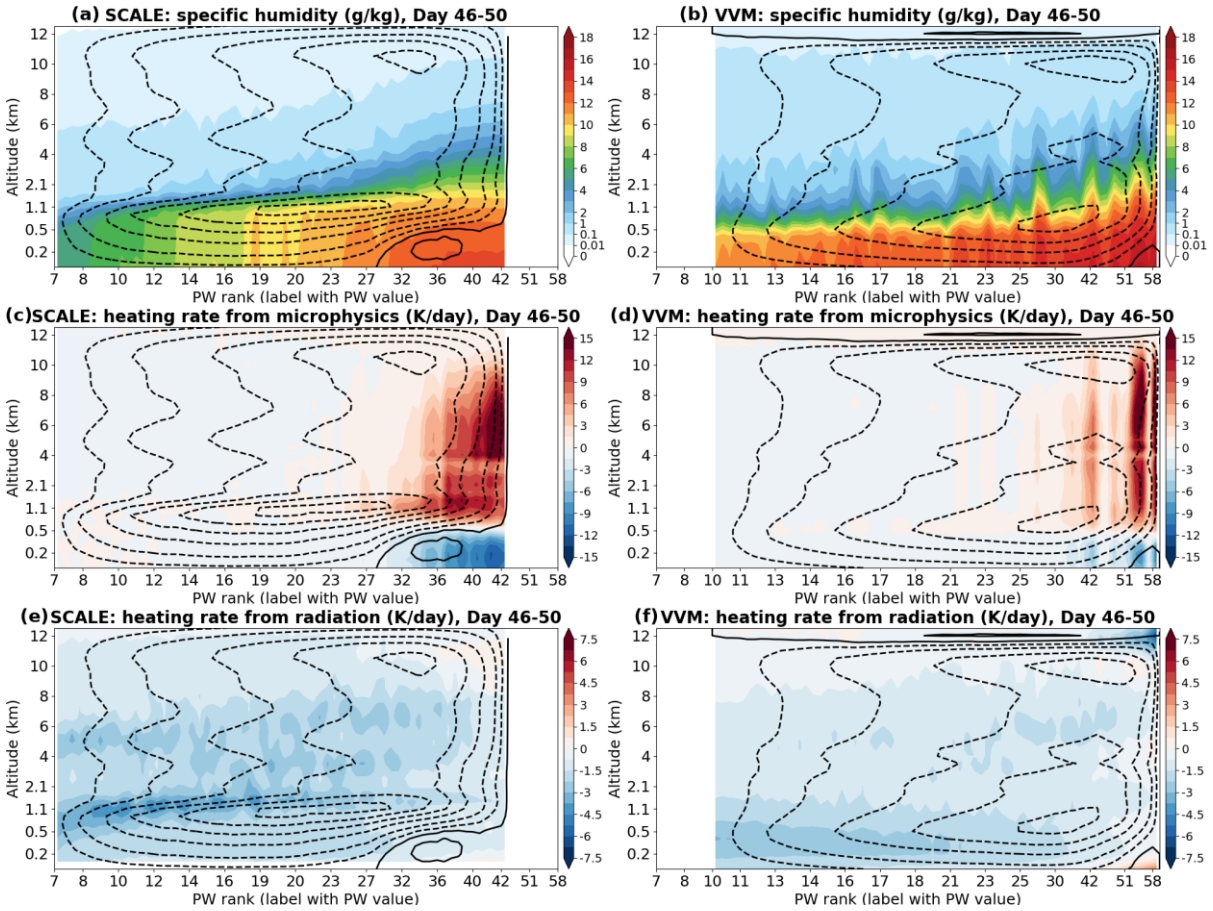

Fig. 2. The vertical profiles of specific humidity (a, b), microphysical latent heating rate (c, d), radiative heating rate (e, f) are ranked by precipitable water with the same sample size in each rank for SCALE (left) and VVM (right) in days 46-50 (Note that the PW range is different for SCALE and VVM). Contours show the streamfunction with intervals of 0.05 kg m^{-2} s^{-1}, and the contours of -0.02 and 0.02 kg m^{-2} s^{-1} are added to show subsidence in drier region and clockwise circulation in the moister region, respectively. The solid and dash lines, respectively, represent clockwise and counterclockwise circulations in the moisture space.

3.2 The self-aggregated states in the moisture space

The characteristics of the aggregation state are evaluated by the vertical profiles ranked by PW (Fig. 2) following Bretherton et al. (2005). After the convective aggregation established, counterclockwise circulations in the moisture space are evident in both models with a narrower

upward branch in the moister region (over 36 mm for SCALE and over 51 mm for VVM) and a wider subsidence region in the drier region (7-23 mm in SCALE and 10-25 mm for VVM). The boundary layer height of SCALE smoothly transits from 1.1 km in the drier region to 2 km in the moister region. In VVM, the boundary layer top is nearly constant at 600 m in the drier region with fluctuations and develops rapidly from roughly 800 m to 2 km in the moister region. Notable differences in the boundary layer are that the counterclockwise circulations of SCALE are stronger and have a gap at the top of the boundary layer, while the shallow circulation of VVM is weaker and smoothly connected with the free-atmospheric circulation. In SCALE, the sharp transition of the circulation at the top of the boundary layer in the drier region corresponds to more significant radiative cooling compared to that of VVM (Fig. 2e and 2f). Above the boundary, the ascending motion occurs with considerable microphysical heating in both models. The condensate heating in SCALE happens in wider areas in the moisture space, while it is confined in the top 10 % moistest areas in VVM. The subsidence region of SCALE accompanies by stronger radiative cooling, while the cooling is very limited in VVM.

The comparison between the two models indicates that the condensate heating in the moister region drives the circulation to effectively export dry static energy to the drier region and maintain self-aggregation. In contrast, the radiative cooling in the drier region contributes to the maintenance of the aggregation in SCALE, and the microphysical heating is relatively less than VVM. This is because the upward motion in VVM occurs in a moister environment than that in SCALE, and the heating could be more efficient in drying the adjacent environment (Hack and Schubert 1986). Interestingly, the difference in the important processes for self-aggregation of two models can be analogous to Coppin and Bony (2015): the SCALE represents the cold mean state where the radiative cooling is the main driver of the aggregation, while VVM represents the warm mean state where deep convection is the main driver.

Although the two models share the same bottom boundary condition, the analyses in the moisture space clarify different contributions are mainly from the radiative process in SCALE and the convective process in VVM.

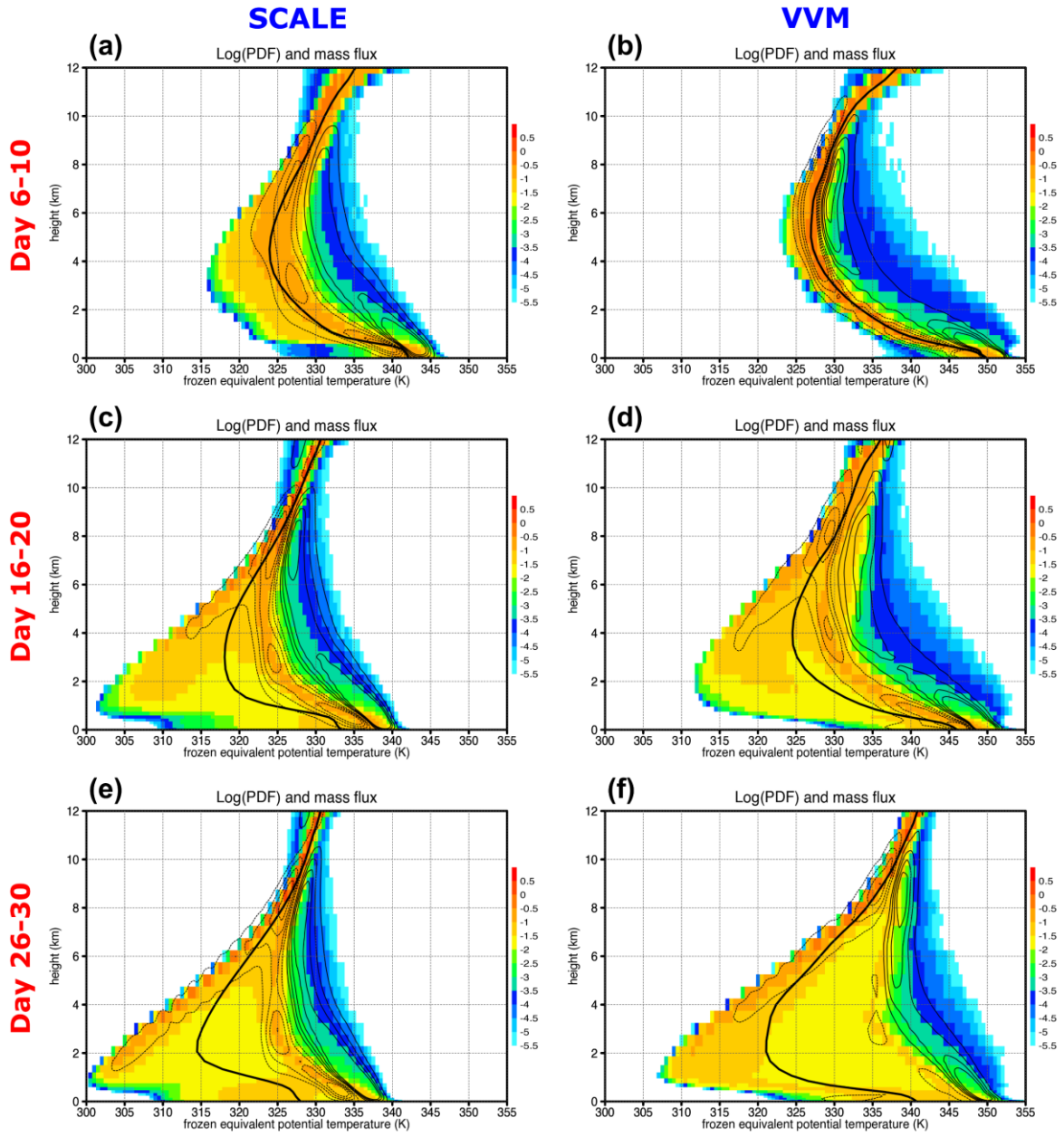

Fig. 3. The isentropic analysis of SCALE (left panels) and VVM (right panels) for day 6-10 (a, b), day 16-20 (c, d), and day 26-30 (e, f). The solid black line represents the mean frozen equivalent potential temperature (θ_{ei}) and the color shading represents the logarithmic probability density function of θ_{ei}. The isentropic mass fluxes are presented by the contours with the interval of 0.003 kg m^{-2} K^{-1}.

3.3 Isentropic analyses on the evolution of aggregation

The different maintenance processes in SCALE and VVM can be traced back to the developing stage of self-aggregation. The isentropic analysis (Pauluis et al. 2013) is applied to evaluate the convective structures via the energetic perspective because of the different contributions of deep convection to self-aggregation in two models. The isentropic distribution is calculated through the conditional sampling by the air parcel's frozen equivalent potential temperature (θ_{ei}, Huang and Wu 2020). The isentropic mass fluxes can be considered as the convective parcels' trajectories on the energy space. In days 6-10, SCALE has a wider isentropic distribution for the altitudes between 1 km and 8 km during days 6-10 because the aggregation starts to develop. In VVM, the aggregation does not develop yet, so the isentropic distribution is close to the domain-averaged θ_{ei} profile. Both models have a local maximum of upward and downward isentropic mass fluxes below 2 km height due to the boundary mixing. The updraft constantly extends from 2 km to 8 km with 5 K changes in θ_{ei} in SCALE. In VVM, the updraft is weak between 2-4 km height with roughly 10 K changes in θ_{ei}, which indicates that convective updraft is greatly influenced by the entrainment. During days 16-20, SCALE and VVM share some similarities on the isentropic diagram as self-aggregation develops commonly. The isentropic distribution shifts toward lower θ_{ei} region due to the development of the dry areas. The noteworthy feature is that an extra subsiding branch of mass flux develops in the region where θ_{ei} is the smallest in each height in 4-6 km. The upward mass fluxes become stronger in the moist region compared to days 6-10 in both models. These changes are found to become more significant during days 26-30 in both models, which could be regarded as the features of the self-aggregation onset. The subsiding mass flux nearby the convective updraft keeps similar strength in SCALE between days 16-20 and days 26-30. This suggests that the convective updraft generates compensating subsidence in the adjacent region, which is similar to the convective-scale circulation in Slawinska et al. (2015). In VVM, the downdraft

close to the updraft is weakened, and the structure of the upward mass flux becomes steeper on days 26-30 than on days 16-20. The circulation that mostly descends in the lowest θ_{ei} region in days 26-30 corresponds to the mesoscale circulation (Slawinska et al. 2015). These results reveal an important fact that the difference in circulation scale is possibly responsible for the difference in the distinct processes for self-aggregation to develop.

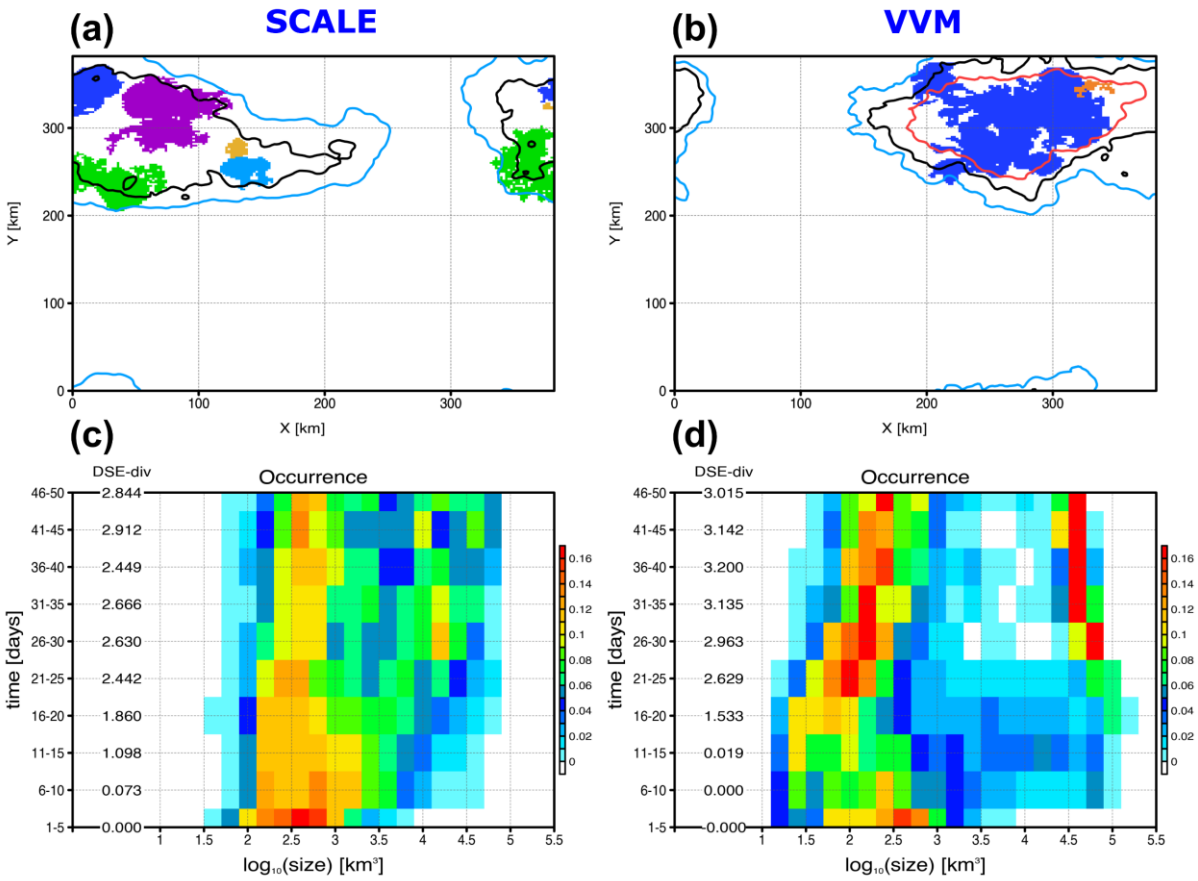

Fig. 4. The surface projections of convective cloud on day 48 for SCALE (a) and VVM (b). Precipitable water of 30, 40, and 50 mm are presented by the cyan, black, and red contours, respectively. Time evolutions of cloud size distribution for SCALE (c) and VVM (d) are shown by the color shading with 5-day intervals. The values with the unit of 10^6 J m^{-2} s^{-1} at the left part of the panels present the temporal averages of column flux divergence of dry static energy (DSE-div) in the moist region where PW is greater than 30 mm.

3.4 The statistics of convective clouds

The object-based analysis (Tsai and Wu 2017) has been used to study the aggregated convection in a different environment and has been used to evaluate the model performance of the precipitation systems (Su et al. 2019). Following their studies, we apply the object-based analysis to evaluate the difference in convection scale between SCALE and VVM. Contiguous

cloudy grids where the total cloud condensates are greater than 10^{-5} kg kg^{-1} are connected and then identified as a convective cloud object using the six-connected segmentation method. Here, we add a condition that the cloud object base is lower than 2 km to ensure convective clouds develop from the boundary layer. Additionally, a criterion that the cloud top height greater than 6 km is used to select the deep convection, which can largely influence the environment and the circulation. The features of convective cloud objects are projected to the surface at day 48 (Fig. 4a and 4b). Both models have a similar coverage of the moist area where precipitable water greater than 30 mm, but the horizontal scales of the convective cloud objects are quite different between SCALE and VVM. Convective cloud objects in SCALE scatter within the moist area with a smaller size. In VVM, the largest cloud object almost occupies the moist area, and some smaller cloud objects surround the largest one. The moist area of VVM is more humid than that of SCALE, and it would support the development of larger convective clouds. The evolution of the size distribution shows that the size of convective clouds tends to be smaller than 10^3 km^3 in both models. As self-aggregation develops, the size distributions in both models become a bimodal distribution with peaks of smaller and larger sizes, and the bimodal distribution in VVM is more obvious than that in SCALE. The large-size peak splits from the small-size peak in days 6-30 and shifts to about 10^4 km^3 gently in SCALE, while the large-size peak in VVM leaps to $10^{4.5}$ km^3 in days 11-25. The convective cloud objects with a size greater than 10^4 km^3 rarely appear in SCALE, while they frequently develop with larger sizes in VVM.

The larger convective clouds mostly covering the moist region in VVM can more efficiently export dry static energy (DSE) to the dry region in the upper troposphere. In contrast, the smaller convective clouds in SCALE lead to the subsidence in the clear-sky region between the convective clouds in SCALE, which corresponds to the subsidence nearby the upward motion on the isentropic diagram. This argument is supported by calculating the divergence of

column-integrated dry static energy (DSE-div) in the moist region where PW larger than 30 mm. DSE-div in both models increases with the emerge of the large-size peak in the size spectrum. The increase of DSE-div accompanies by the gentle shift of the large-size peak in SCALE, while DSE-div rapidly grows in days 11-25 in VVM when the size distribution sharply transits. After day 30, the export of DSE in the moist region in VVM is greater than that in SCALE because the larger convective clouds frequently develop. These results indicate that the larger convective clouds in VVM can efficiently drive the circulation and hence the development of self-aggregation.

4 Summary and Discussion

In this study, RCE simulations are conducted using two CRMs (SCALE and VVM) following the RCEMIP protocol (Wing et al. 2020), and the setups of the horizontal domain and resolution are adopted from Yanase et al. (2020). The development of self-aggregation is mainly focused to examine the critical process for self-aggregation. Even though the two models reach a self-aggregation state after 40 days of the simulations, the pathways toward aggregation are very different. The dry area expansion and the moist area shrink are evident in SCALE through radiative effects, while VVM takes a different route through the convection development in the moist region. The analyses in the moisture space show that self-aggregation in SCALE develops through the strong shallow circulation induced by the enhanced radiative cooling near the boundary layer top. The isentropic analysis shows that the subsidence induced by the organized convection in VVM further enhances the expansion of the dry region and leads to self-aggregation. The pathways to self-aggregation in SCALE and VVM are, respectively, similar to the mechanisms in cold and warm SST scenarios in Coppin and Bony (2015). In their study, the critical mechanism for the development of self-aggregation depends on the mean state determined by SST. Our results highlight that even though both models reach a similar equilibrium state with the same SST of 300 K, the transition toward self-aggregation is different between SCALE and VVM. It is found that the size of convective clouds is responsible for the difference in the ability to drive the mesoscale circulation, which results in the different pathways to self-aggregation.

The different pathways to self-aggregation between SCALE and VVM imply that the climate sensitivity represented by those models would be different. In SCALE, self-aggregation develops due to strong radiative cooling, which could largely alter the radiative energy budget. Self-aggregation with enhanced longwave cooling in the dry areas can largely

offset the warming due to the imbalance of radiative forcing such as the greenhouse gases. As radiative cooling dominates the development of self-aggregation, the climate sensitivity would be smaller in SCALE. On the other hand, self-aggregation develops due to the organization process of convection, and the radiative feedback is relatively inefficient in VVM. These results suggest that the changes in convective structures are the primary response to the warming climate, and the climate sensitivity would be larger in VVM. The variabilities among CRMs in RCEMIP could result in the spread of the climate sensitivity, which is worth further investigations in the future.

Acknowledgments

We thank Prof. Wei-Ting Chen for providing valuable discussions on this study. Jin-De Huang and Chien-Ming Wu were supported by Taiwan's MoST through Grant 107-2111-M-002-010-MY4 and Academia Sinica through Grant AS-TP-109-M11 to National Taiwan University. Ching-Shu Hung and Hiroaki Miura were supported by JSPS KAKENHI Grant Number JP16H04048 and JP20H05729. The two models used in this study can be obtained from https://scale.riken.jp/ (SCALE, version 5.3.6) and https://doi.org/10.6084/m9.figshare.14866260.v1 (VVM, version 1.5.1). The analyzing codes and post-processing data are available in the online open access repository (https://doi.org/10.6084/m9.figshare.11933091.v3).

References

Arakawa, A., & Wu, C.-M. (2013). A unified representation of deep moist convection in numerical modeling of the atmosphere. Part I. Journal of the Atmospheric Sciences, 70(7), 1977–1992. https://doi.org/10.1175/JAS-D-12-0330.1

Beljaars, A. C. M., & Holtslag, A. A. M. (1991). Flux parameterization over land surfaces for atmospheric models. Journal of Applied Meteorology, 30(3), 327–341. https://doi.org/10.1175/1520-0450(1991)030<0327:FPOLSF>2.0.CO;2

Bretherton, C. S., Blossey, P. N., & Khairoutdinov, M. (2005). An energy-balance analysis of deep convective self-aggregation above uniform SST. Journal of the Atmospheric Sciences, 62, 4273–4292. https://doi.org/10.1175/JAS3614.1

Brown, A. R., Derbyshire, S. H., & Mason, P. J. (1994). Large-eddy simulation of stable atmospheric boundary layers with a revised stochastic subgrid model. Quarterly Journal of the Royal Meteorological Society, 120(520), 1485–1512. https://doi.org/10.1002/qj.49712052004

Chang, Y.-H., Chen, W.-T., Wu, C.-M., Moseley, C., & Wu, C.-C. (2021). Tracking the influence of cloud condensation nuclei on summer diurnal precipitating systems over complex topography in Taiwan. Atmospheric Chemistry and Physics. Discuss. https://doi.org/10.5194/acp-2021-113

Chen, F., & Dudhia, J. (2001). Coupling an Advanced Land Surface–Hydrology Model with the Penn State–NCAR MM5 Modeling System. Part I: Model Implementation and Sensitivity. Monthly Weather Review, 129(4), 569-585. https://doi.org/10.1175/1520-0493(2001)129<0569:CAALSH>2.0.CO;2

Chen, Y.-T., & Wu, C.-M. (2019). The role of interactive SST in the cloud-resolving simulations of aggregated convection. Journal of Advances in Modeling Earth Systems, 11, 3321–3340. https://doi.org/10.1029/2019MS001762

Chen, W.-T., Wu, C.-M., Tsai, W.-M., Chen, P.-J., & Chen, P.-Y. (2019). Role of coastal convection to moisture buildup during the South China Sea summer monsoon onset. Journal of the Meteorological Society of Japan, 97(6), 1155-1171. https://doi.org/10.2151/jmsj.2019-065

Chien, M.-H., & Wu, C.-M. (2016). Representation of topography by partial steps using the immersed boundary method in a vector vorticity equation model (VVM). Journal of Advances in Modeling Earth Systems, 8, 212–223. https://doi.org/10.1002/2015MS000514

Coppin, D., & Bony, S. (2015). Physical mechanisms controlling the initiation of convective self-aggregation in a General Circulation Model. Journal of Advances in Modeling Earth Systems, 7, 2060–2078. https://doi.org/10.1002/2015MS000571

Held, M. I., Hemler, R. S., & Ramaswamy, V. (1993). Radiative-convective equilibrium with explicit two-dimensional moist convection. Journal of the Atmospheric Sciences, 50, 3909–3927. https://doi.org/10.1175/1520-0469(1993)050%3C3909:RCEWET%3E2.0.CO;2

Hack, J. J., & Schubert, W. H. (1986). Nonlinear Response of Atmospheric Vortices to Heating by Organized Cumulus Convection, Journal of Atmospheric Sciences, 43(15), 1559-1573. https://doi.org/10.1175/1520-0469(1986)043<1559:NROAVT>2.0.CO;2

Huang, J.-D., & Wu, C.-M. (2020). Effects of microphysical processes on the precipitation Spectrum in a strongly forced environment. Earth and Space Science, 7, e2020EA001190. https://doi.org/10.1029/2020EA001190

Iacono, M. J., Delamere, J. S., Mlawer, E. J., Shephard, M. W., Clough, S. A., & Collins, W. D. (2008), Radiative forcing by long-lived greenhouse gases: Calculations with the

AER radiative transfer models. Journal of Geophysical Research, 113, D13103. https://doi.org/10.1029/2008JD009944

Jung, J.-H., & Arakawa, A. (2008). A three-dimensional anelastic model based on the vorticity equation. Monthly Weather Review., 136(1), 276–294. https://doi.org/10.1175/2007MWR2095.1

Kuo, K.-T., & Wu, C.-M. (2019). The precipitation hotspots of afternoon thunderstorms over the Taipei Basin: Idealized numerical simulations. Journal of the Meteorological Society of Japan, 97(2), 501–517. https://doi.org/10.2151/jmsj.2019-031

Manabe, S., & Strickler, R. F. (1964). Thermal Equilibrium of the Atmosphere with a Convective Adjustment, Journal of Atmospheric Sciences, 21(4), 361-385. https://doi.org/10.1175/1520-0469(1964)021<0361:TEOTAW>2.0.CO;2

Morrison, H., & Milbrandt, J. A. (2015). Parameterization of ice microphysics based on the prediction of bulk particle properties. Part I: Scheme description and idealized tests. Journal of the Atmospheric Sciences, 72, 287–311. https://doi.org/10.1175/JAS-D-14-0065.1

Muller, C. J., & Held, I. M. (2012). Detailed Investigation of the Self-Aggregation of Convection in Cloud-Resolving Simulations, Journal of the Atmospheric Sciences, 69(8), 2551-2565. https://doi.org/10.1175/JAS-D-11-0257.1

Nakajima, K., & Matsuno, T. (1988). Numerical experiments concerning the origin of cloud clusters in the tropical atmosphere. Journal of the Meteorological Society of Japan, 66, 309-329. https://doi.org/10.2151/jmsj.81.713

Nishizawa, S., Yashiro, H., Sato, Y., Miyamoto, Y., & Tomita, H. (2015). Influence of grid aspect ratio on planetary boundary layer turbulence in large-eddy simulations.

Geoscientific Model Development, 8(10), 3393–3419. https://doi.org/10.5194/gmd-8-3393-2015

Pauluis, O., & Mrowiec, A. A. (2013). Isentropic analysis of convective motions. Journal of the Atmospheric Sciences, 70, 3673–3688. https://doi.org/10.1175/JAS-D-12-0205.1

Sato, Y., Nishizawa, S., Yashiro, H., Miyamoto, Y., Kajikawa, Y., & Tomita, H. (2015). Impacts of cloud microphysics on trade wind cumulus: Which cloud microphysics processes contribute to the diversity in a large eddy simulation? Progress in Earth and Planetary Science, 2(1), 23. https://doi.org/10.1186/s40645-015-0053-6

Scotti, A., Meneveau, C., & Lilly, D. K. (1993). Generalized Smagorinsky model for anisotropic grids. Physics of Fluids A: Fluid Dynamics, 5(9), 2306–2308. https://doi.org/10.1063/1.858537

Sekiguchi, M., & Nakajima, T. (2008). A k-distribution-based radiation code and its computational optimization for an atmospheric general circulation model. Journal of Quantitative Spectroscopy and Radiative Transfer, 109(17–18), 2779–2793. https://doi.org/10.1016/j.jqsrt.2008.07.013

Slawinska, J., Pauluis, O., Majda, A. J., & Grabowski, W. W. (2016). Multiscale Interactions in an Idealized Walker Cell: Analysis with Isentropic Streamfunctions. Journal of the Atmospheric Sciences, 73(3), 1187-1203. https://doi.org/10.1175/JAS-D-15-0070.1

Su, C.-Y., Wu, C.-M., & Chen, W.-T. (2019). Object-based precipitation system bias in grey zone simulation: the 2016 South China Sea summer monsoon onset. Climate Dynamics, 53, 617–630. https://doi.org/10.1007/s00382-018-04607-x

Tomita, H. (2008). New microphysical schemes with five and six categories by diagnostic generation of cloud ice. Journal of the Meteorological Society of Japan, 86A, 121–142. https://doi.org/10.2151/jmsj.86A.121

Tompkins, A. M., & Craig, G. C. (1998). Radiative-convective equilibrium in a three-dimensional cloud-ensemble model. Quarterly Journal of the Royal Meteorological Society, 124, 2073–2097. https://doi.org/10.1002/qj.49712455013

Tsai, J.-Y., & Wu, C.-M. (2016). Critical transitions of stratocumulus dynamical systems due to perturbation in free atmosphere moisture. Dynamics of Atmospheres and Oceans, 76, 1–13. https://doi.org/10.1016/j.dynatmoce.2016.08.002

Tsai, W.-M., & Wu, C.-M. (2017). The environment of aggregated deep convection. Journal of Advances in Modeling Earth Systems, 9, 2061–2078, https://doi.org/10.1002/2017MS000967.

Wilson, K. D. (2001). An alternative function for the wind and temperature gradients in unstable surface layers. Boundary-Layer Meteorology, 99(1), 151–158. https://doi.org/10.1023/A:1018718707419

Wing, A. A., & Emanuel, K. (2014). Physical mechanisms controlling self-aggregation of convection in idealized numerical modeling simulations. Journal of Advances in Modeling Earth Systems, 6, 59–74. https://doi.org/10.1002/2013MS000269

Wing, A. A., Reed, K. A., Satoh, M., Stevens, B., Bony, S., & Ohno, T. (2018). Radiative-Convective Equilibrium Model Intercomparison Project. Geoscientific Model Development, 11, 793–813. https://doi.org/10.5194/gmd-11-793-2018

Wing, A. A., Stauffer, C. L., Becker, T., Reed, K. A., Ahn, M.-S., & Arnold, N. P., et al. (2020). Clouds and convective self-aggregation in a multimodel ensemble of radiative-convective equilibrium simulations. Journal of Advances in Modeling Earth Systems, 12(9), 1942-2466. https://doi.org/10.1029/2020MS002138

Wu, C.-M., & Arakawa, A. (2011). Inclusion of surface topography into the vector vorticity equation model (VVM). Journal of Advances in Modeling Earth Systems, 3, M04002. https://doi.org/10.1029/2011MS000061

Wu, C.-M., & Arakawa, A. (2014). A unified representation of deep moist convection in numerical modeling of the atmosphere. Part II. Journal of the Atmospheric Sciences, 71(6), 2089–2103. https://doi.org/10.1175/JAS-D-13-0382.1

Wu, C.-M., Lin, H.-C., Cheng, F.-Y., & Chien, M.-H. (2019). Implementation of the land surface processes into a vector vorticity equation model (VVM) to study its impact on afternoon thunderstorms over complex topography in Taiwan. Asia-Pacific Journal of Atmospheric Sciences. https://doi.org/10.1007/s13143-019-00116-x

Wu, C.-M., & Chen, P.-Y. (2021). Idealized cloud-resolving simulations of land-atmosphere coupling over tropical islands. Terrestrial, Atmospheric and Oceanic sciences journal, in press. https://doi.org/ 10.3319/TAO.2020.12.16.01

Yanase, T., & Takemi, T. (2018). Diurnal variation of simulated cumulus convection in radiative-convective equilibrium. Scientific Online Letters on the Atmosphere, 14, 116-120. https://doi.org/10.2151/sola.2018-020

Yanase, T., Nishizawa, S., Miura, H., Takemi, T., & Tomita, H. (2020). New critical length for the onset of self-aggregation of moist convection. Geophysical Research Letters, 47, e2020GL088763. https://doi.org/10.1029/2020GL088763